Structure-Based Optimization of Azole Antifungal Agents by CoMFA, CoMSIA, and Molecular Docking

Chunquan Sheng, Wannian Zhang,* Haitao Ji, Min Zhang, Yunlong Song, Hui Xu, Jie Zhu, Zhenyuan Miao, Qingfen Jiang, Jianzhong Yao, Youjun Zhou, Jü Zhu, and Jiaguo Lü

School of Pharmacy, Second Military Medical University, 325 Guohe Road, Shanghai 200433, People's Republic of China

Received December 1, 2005

In a continuing effort to develop highly potent azole antifungal agents, the three-dimensional quantitative structure−activity relationship methods, CoMFA and CoMSIA, were applied using a set of novel azole antifungal compounds. The binding mode of the compounds at the active site of lanosterol 14α-demethylase was further explored using the flexible docking method. Various hydrophobic, van der Waals, $\pi-\pi$ stacking, and hydrogen bonding interactions were observed between the azoles and the enzyme. Based on results from the molecular modeling, a receptor-based pharmacophore model was established to guide the rational optimization of the azole antifungal agents. Thus, a total of 57 novel azoles were designed and synthesized by a three-step optimization process. In vitro antifungal assay revealed that the antifungal activities of these novel azoles were greatly improved, which confirmed the reliability of the model from molecular modeling.

Introduction

During the past two decades, the life threatening infections caused by pathogenic fungi have become increasingly common, especially in individuals with immunocompromised hosts, such as patients undergoing anticancer chemotherapy or organ transplants and patients with AIDS.[1] Clinically, candidosis, aspergillosis and cryptococcosis are three major fungal infections in immunocompromised individuals.[2,3] Moreover, dermatomycoses, such as toenails and tinea pedis, are among the most widespread human superficial and cutaneous fungal infections. However, the current antifungal therapy suffers from drug related toxicity, severe drug resistance, nonoptimal pharmacokinetics, and serious drug−drug interactions. Therefore, there is an emergent need to develop novel antifungal drugs with higher efficiency, broader spectrum, and lower toxicity.

The common antifungal agents currently used in clinic are azoles (such as fluconazole, ketoconazole, and itraconazole),[4] polyenes (such as amphotericin B[5] and nystatin[6]), echinocandins (such as caspofungin and micafungin),[7] and allylamines (such as naftifine and terbinafine).[8] Among those, azoles have fungistatic, orally active, and broad-spectrum activities against most yeasts and filamentous fungi. They are widely used in antifungal chemotherapy. Fluconazole shows good antifungal activity with relatively low toxicity and is preferred as first-line antifungal therapy.[9] However, fluconazole is not effective against invasive aspergillosis and has suffered severe drug resistance.[10;11] Itraconazole is an improvement of fluconazole in terms of having a broader antifungal spectrum and better toleration. However, its use is hampered by variable oral absorption and low bioavailability. This situation has led to an ongoing search for new azoles, and several novel azoles have been developed with improved profiles. The second generation of azoles (Chart 1), such as voriconazole,[12] posaconazole,[13] and ravuconazole,[14] are marketed or currently in the late stages of clinical trials. They are noted for their broad antifungal spectrum, low toxicity, and improved pharmacodynamic profiles.

Azole antifungals act by competitive inhibition of the lanosterol 14α-demethylase ($P450_{14DM}$, CYP51), the enzyme that catalyzes the oxidative removal of the 14α-methyl group of lanosterol to give $\Delta^{14,15}$-desaturated intermediates in ergosterol biosynthesis.[15] In yeast and fungi, CYP51 is the key enzyme in sterol biosynthesis. Selective inhibition of CYP51 would cause depletion of ergosterol and accumulation of lanosterol and other 14-methyl sterols resulting in the growth inhibition of fungal cells.[16] Due to the importance of CYP51 in antifungal drug studies, it is of great importance to know the three-dimensional (3D) structures of CYP51s, particularly, the CYP51s from pathogenic fungi. However, eukaryotic CYP51s are membrane-associated proteins, and solving their crystal structures remains a challenge. In our previous studies,[17] we have constructed a 3D model of CYP51 from *Candida albicans* (CACYP51) through homology modeling on the basis of the crystallographic coordinates of four prokaryotic P450s: P450BM3,[18] P450cam,[19] P450terp,[20] and P450eryF.[21] The pharmacophoric conformation of azole antifungal agents was searched by the active analogue approach and then docked into the active site of the enzyme. Subsequently, the active site of the modeled structure was investigated by MCSS functional group mapping and LUDI calculations. Several non-azole lead compounds were designed and synthesized by structure-based de novo design approach.[22] The designed lead compounds exhibited a strong inhibitory effect on CYP51 of *C. albicans*, but they only showed marginal antifungal activity in vitro as compared to fluconazole. The low structural identity between the prokaryotic P450s and the eukaryotic CYP51s limits the development of highly potent inhibitors and led us to build a more accurate model of CYP51 from pathogenic fungi.

In 2001, Podust et al. reported the crystal structure of a prokaryotic sterol 14α-demethylase from *Mycobacterium tuberculosis* (MTCYP51), in complex with two azole inhibitors (4-phenylimidazole and fluconazole), which is the only crystal structure for the CYP51 family.[23] More recently, estriol bound and ligand free structures of MTCYP51 were also reported.[24] Although this crystal structure of CYP51 was not from fungi, it can provide a more accurate structural template for modeling the 3D structures of fungal CYP51 than the prokaryotic P450s. For this purpose, we rebuilt the 3D model of CYP51 from *C. albicans* and *Aspergillus fumigatus* on the basis of the crystal

* To whom correspondence should be addressed. Phone: 86-21-25074460. Fax: 86-21-25074460. E-mail: zhangwnk@hotmail.com.

10.1021/jm051211n CCC: $33.50
Published on Web 03/22/2006

Chart 1

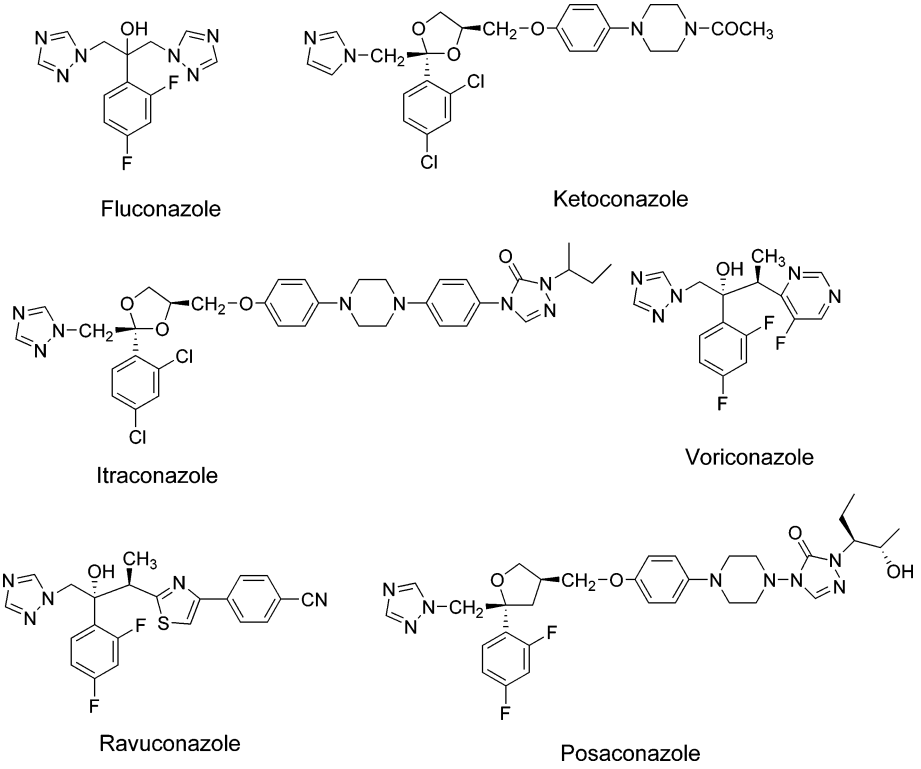

coordinates of MTCYP51. The binding mode of the substrate with fungal CYP51 was also investigated.[25] In a continuing effort to find more potent azole antifungal agents and design lead compounds with higher affinity, we have designed a series of novel azoles with substituted piperazinyl side chains. These new azoles exhibited better antifungal activity in vitro than fluconazole and itraconazole.[26;27] These compounds can be used as a reliable data set to perform computational simulations to gain insights into the structural and chemical features required for the antifungal activity.

Although extensive efforts have been put to the structural modification of current azole antifungals,[28,29] most of them were undertaken only by traditional methods, which was time-consuming and less effective. The structural information of the target enzyme can be utilized to accelerate the discovery of novel antifungal agents. Several three-dimensional quantitative structure−activity relationship (3D-QSAR) studies for different azole antifungals have been reported.[28,30−33] However, most of these models did not incorporate the structural information of the receptor, and the robustness of the models remained to be confirmed by further drug design and synthesis. Also, a number of docking analysis studies of current azole antifungal agents have been performed,[34−38] but these papers paid more attention to the mechanism of drug resistance and the selectivity between candidosis and aspergillosis. In the present study, we applied comparative molecular field analysis (CoMFA)[39] and comparative molecular similarity indices analysis (CoMSIA)[40] based on a set of novel azole antifungals from our laboratory to build robust 3D-QSAR models. The binding mode of these compounds was further clarified by molecular docking. On the basis of the results from 3D-QSAR and docking, a pharmacophore model for the rational optimization of azole antifungal agents was constructed. Novel antifugal azoles were then designed and synthesized according to the developed pharmacophore model, which exhibited excellent antifungal activity with broad antifungal spectrum.

Chemistry

The synthesis of all compounds in the data set (**1**−**40**) has been published previously.[26,27] All the target compounds synthesized that possess a chiral center on the C2 atom are racemates. As a key intermediate of our designed triazole antifungals, the oxirane compound **44** was synthesized by an improved procedure by this labratory.[41] The preparation of trizoles with benzylamine side chains (compounds **45**−**57**) is outlined in Scheme 1. The title compounds **45**−**57** were prepared by ring-open reaction of epoxide **44** with various *N*-methyl benzylamines, which were obtained by the reported methods.[42] This reaction proceeded better in the protic solvent (such as ethanol) than in nonprotic solvents. The triazoles with amide-benzylamine side chains (compounds **58**−**67**) were synthesized starting from compound **57**, using conventional methods as depicted in Scheme 2. The good yields were obtained when these reactions were performed in dichloromethane in the presence of a base at room temperature. Triethylamine is a better base than either potassium carbonate or sodium hydroxide. The triazoles with triazolone-benzylamine side chains (compounds **76**−**109**) were synthesized via eight steps (Scheme 3). The amino group of compound **68** was first protected by $(BOC)_2O$. Then the nitro group on the phenyl ring was reduced to an amino group in the presence of Raney Ni and hydrazine hydrate. In the presence of a base at room temperature, the aniline **70** was converted to phenylcarbamate **71** by reacting with phenyl chloroformate. Using pyridine as the base and ethyl acetate as the solvent results in a better yield than the combination of triethylamine (base) and dichloromethane (solvent). Phenylcarbamate **71** was treated with hydrazine hydrate to give semicarbazide **72**, which was subsequently reacted with formamidine acetate in the presence of DMF at 80 °C to give the triazolone **73**. Triazolone **73** was treated with substituted benzyl chlorides and substituted 2-chloro-1-phenyl-ethanones in the presence of potassium carbonate and DMF at 80 °C to afford various protected triazolone-benzyl-

Scheme 1

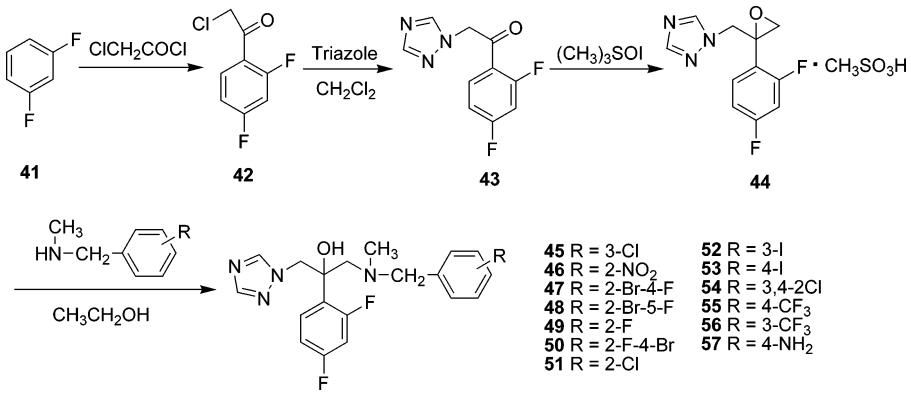

Scheme 2

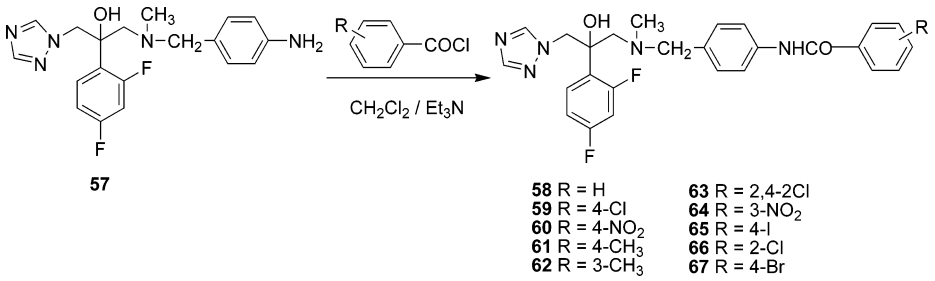

amines, which were then deprotected by 10% HCl in ethyl acetate to give triazolone-benzylamine side chains. The target compounds **76**−**109** were obtained by treating epoxide **44** with various triazolone-benzylamine side chains in the presence of triethylamine and ethanol at 80 °C with moderate to high yields.

Results and Discussions

CoMFA and CoMSIA Models. A data set of our newly synthesized triazole antifungal agents was used to perform the 3D-QSAR studies. The antifungal activities of the compounds were all determined utilizing the same experimental protocol in our laboratory, covered a range of 3 orders of magnitude, and uniformly distributed. During the optimization of 3D-QSAR models, variations of parameters, such as grid spacing and attenuation factor, were considered. However, the best results were obtained from the parameters with the default values. It has been discussed that the five different descriptor fields are not totally independent of each other and such dependencies of individual fields usually decrease the statistical significance of the models.[43,44] An evaluation, which of the five CoMSIA fields are actually needed for a predictive model, was performed by calculating all possible combinations of fields, and the much faster SAMPLS[45] algorithm was used (Figure 2). The first five models, using a single CoMSIA field, indicated that electrostatic field and hydrophobic field were more important than the other three fields. The combination of electrostatic and hydrophobic field gave the best two-field model ($q^2_{SAMPLS} = 0.652$). The addition of steric field resulted in the slight increase of q^2_{SAMPLS} value, and the combination of steic, electrostatic, and hydrophobic fields was proved to be the best model ($q^2_{SAMPLS} = 0.655$).

As shown in Figure 1 and Table 1, compounds in the data set were used as racemates for antifungal testing. CoMFA and CoMSIA studies performed on both *R* and *S* isomers of the compunds were also considered. In most cases, there are three possibilities when the enantiomers affect the bioactvity. First, the two isomers have the same activity, and the activities from the racemates are suitable for the 3D-QSAR studies. Second, one enantiomer is active while the other is completely inactive. Thus, the activities of the racemates should be doubled when we build 3D-QSAR models on single enantiomers. Third, both enantiomers have activities but one enantiomer is more active. In this case, the activities of the enantiomers are difficult to be determined when we only have data from the racemates. However, the use of the doubled values of the biological data should be an alternative way. In the present studies, the 3D-QSAR calculations were repeated on both *R* and *S* isomers of the compounds with their MIC_{80} values doubled. However, only minor changes in the statistical parameters were observed, and the original MIC_{80} values for the racemates were used to build the final CoMFA and CoMSIA models.

A correlation coefficient of $r^2 = 0.940$ and 0.952 and a cross-validated coefficient of $q^2 = 0.718$ and 0.655 were obtained for the best CoMFA and CoMSIA model, respectively (Table 2). The final CoMFA and CoMSIA models were satisfactory from the viewpoint of the statistical significance and the predictive ability of the training set and test set (see Table 1, Figures 3 and 4). However, the ultimate test for the usefulness of a 3D-QSAR model in the drug design process is to predict the activity of new compounds that are not included in the data set. Therefore, we designed and synthesized a test set comprising 57 novel triazole antifungal compounds on the basis of the results from 3D-QSAR and molecular docking studies, which is discussed below.

CoMFA and CoMSIA Contour Maps. To visualize the information content of the derived 3D-QSAR models, CoMFA and CoMSIA contour maps were generated. The field energies at each lattice point were calculated as the scalar results of the coefficient and the standard deviation associated with a particular column of the data table ("stdev*coeff"), which was always plotted as the percentage of the contribution to the CoMFA or CoMSIA equation. Because most structural modifications of azole antifungal agents were aimed to change the side chains attached to C3, the contour plots around the substitutions on

Scheme 3

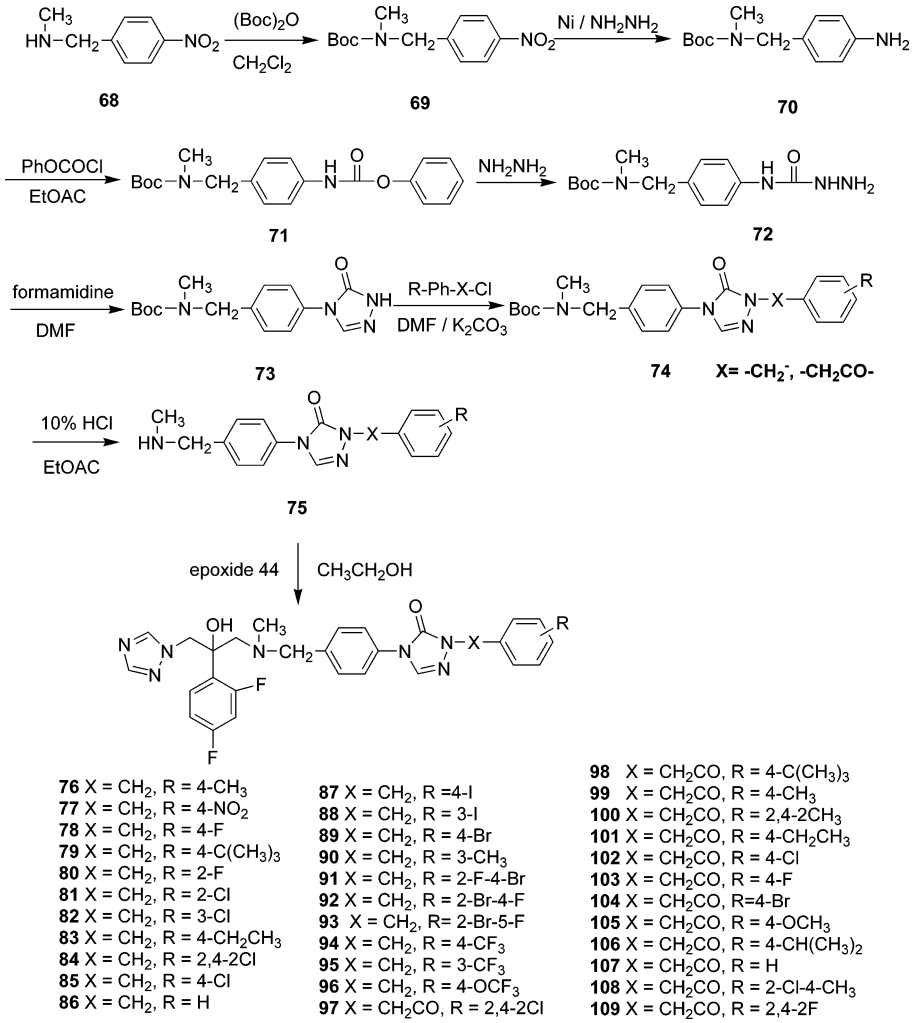

the piperazinyl side chain could reflect the properties of the corresponding region in the active site of CACYP51 and could guild the rational optimization of the azoles in the data set.

Because CoMFA and CoMSIA contour maps of steric and electrostatic fields revealed similar results, only CoMFA contour maps are shown. In Figure 5, the CoMFA contour map of steric field is displayed. The green contours represent the regions of high steric tolerance, while yellow contours represent regions of unfavorable steric effects. The sterically favored regions are around the ortho-position and para-position of the phenyl ring, which indicates that compounds with larger substitutions are essential for high antifungal activity. For example, the substitutions on the para-position of the phenyl group of compounds **27**, **34**, and **22** are methyl, ethyl, and *tert*-butyl, respectively, and the bulkier substitutions lead to more active compounds. There is a small sterically disfavored region around the meta-position of the phenyl ring, and this result can be understood in considering the higher antifungal activity of compound **24** than that of compound **36**. Negatively charged (electron-rich) favorable red regions are found at ortho- and para-positions of the phenyl (Figure 6), indicating that an electron-withdrawing substituent enhances the activity. These regions support the observation that compound **1**, **2**, and **3** with electron-rich substitution at the ortho-position are among the compounds with highest antifungal activity. A blue region around the linker between phenyl and piperazinyl represents an area where positive charge is favored (Figure 6). This result is in good agreement with the fact that the benzoyl analogues showed lower

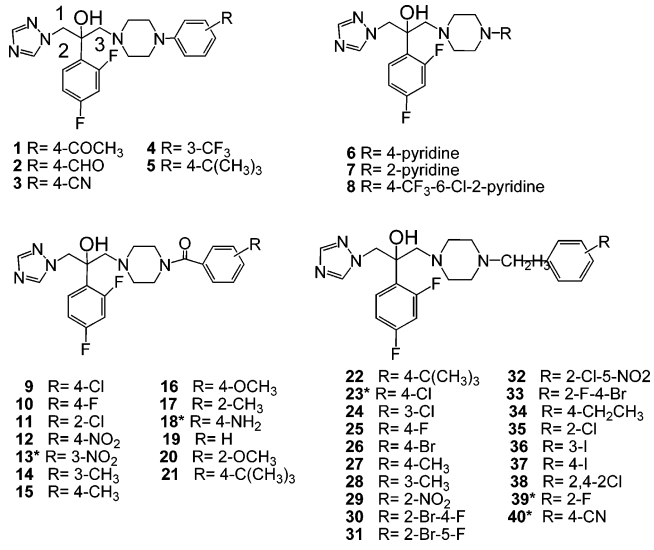

Figure 1. Structure of the compounds in the training set and test set (asterisk indicates compounds in test set).

antifungal activity than the other compounds and the negative charge of the carbonyl is disfavored for the antifungal activity.

Furthermore, CoMSIA reveals other contour maps that are not shown by CoMFA. Cyan regions in Figure 7 indicate areas where hydrophobic substitutions are preferred, and hydrophobic disfavored regions are not shown with contribution level of 20%.

Table 1. Experimental and Calculated Antifungal Activity (−log MIC_{80}) of Compounds in the Training Set and the Test Set for the Final CoMFA and CoMSIA Models

compd	obsd	CoMFA calcd	CoMSIA calcd	compd	obsd	CoMFA calcd	CoMSIA calcd
1	1.470	1.371	1.540	**21**	−0.015	0.291	−0.090
2	1.456	1.500	1.519	**22**	1.469	1.584	1.328
3	1.490	1.389	1.396	**23**[a]	1.447	1.534	1.878
4	1.495	1.429	1.466	**24**	0.855	0.740	0.917
5	0.863	0.806	0.856	**25**	0.237	0.706	0.633
6	−0.398	−0.928	−0.414	**26**	0.596	0.694	0.714
7	0.807	0.753	0.812	**27**	−0.369	−0.316	−0.111
8	0.906	1.117	0.847	**28**	0.534	0.421	0.274
9	0.267	−0.152	−0.069	**29**	−1.543	−1.328	−1.544
10	−0.349	−0.087	−0.042	**30**	0.912	0.862	1.050
11	−0.335	−0.655	−0.347	**31**	0.912	0.638	0.666
12	−0.025	0.136	−0.048	**32**	0.596	0.512	0.596
13[a]	−1.229	−1.137	−1.318	**33**	1.213	1.362	1.334
14	−0.355	−0.437	−0.384	**34**	0.247	−1.101	−0.055
15	−0.258	−1.172	−0.774	**35**	0.253	0.289	0.367
16	0.564	0.620	0.549	**36**	0.635	0.701	0.860
17	−1.559	−1.016	−1.368	**37**	0.936	0.890	1.016
18[a]	−1.558	−1.532	−1.379	**38**	1.480	1.390	1.313
19	−0.369	−0.705	−0.766	**39**[a]	−0.666	−0.502	−0.624
20	−1.243	−1.226	−1.363	**40**[a]	0.545	0.428	0.387

Table 2. Statistical Parameters for the Final CoMFA and CoMSIA Models

						fraction		
model	q^2	r^2	standard error	F	n	steric	electrosatic	hydrophobic
CoMFA	0.718	0.940	0.234	90.838	5	0.334	0.666	
CoMSIA	0.655	0.952	0.204	50.621	5	0.208	0.387	0.405

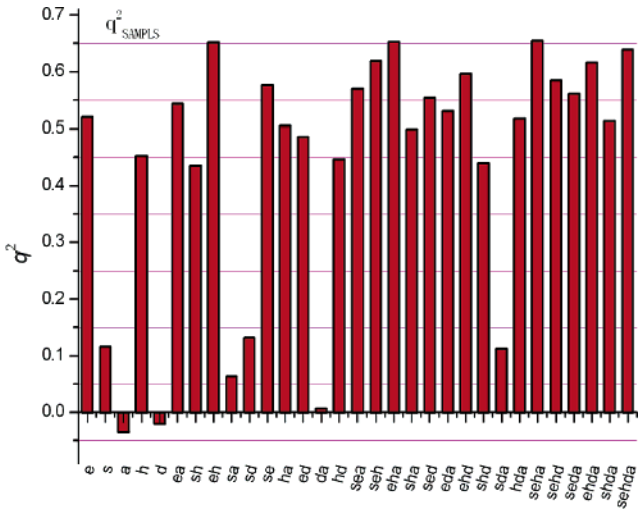

Figure 2. Results of 31 possible CoMSIA field combinations (s = steric, e = electrostatic, h = hydrophobic, d/a = H-bond donor/acceptor) using q^2_{SAMPLS}.

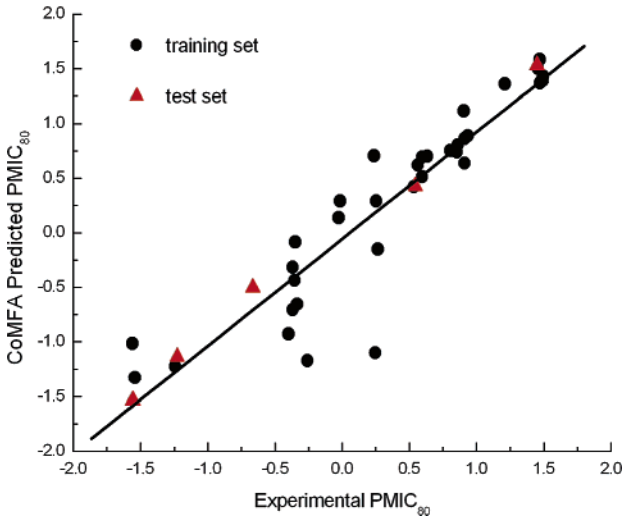

Figure 3. Experimental and calculated $pMIC_{80}$ for the CoMFA analysis of the training set and test set.

The hydrophobic favored regions are around the ortho-position and para-position of the phenyl ring, which is similar to the steric favored regions. In fact, some steric groups are always hydrophobic. A comparison of compound **25** and **30** (also compound **26** and **33**) shows that the addition of a halogen on the ortho-position of benzyl results in the increase of the antifungal activity, which may be due to the increase in hydrophobicity. Moreover, all the compounds with hydrophobic *tert*-butyl substitution at the para-position of the phenyl ring (compounds **5**, **21**, and **22**) showed high antifungal activity.

Analysis of CoMFA and CoMSIA contour plots revealed that the substitutions on the para-position of the phenyl ring are more important for the antifungal activity than those on the ortho-position and meta-position. For the substitutions on the para-position, the steric and hydrophobic groups or the electro-rich groups are favored, which is further supported by the docking analysis below. For the substitutions on the ortho-position, steric, hydrophobic, and electro-rich groups (e.g. halogens) were favored. The substitutions on the meta-position of the phenyl are not important for the antifungal activity, and it was suitable to leave this position unsubstituted.

Binding Mode of the Azoles. Because 3D-QSAR is only a kind of ligand-based approach, the robustness of the derived models is greatly affected by the diversity of the molecules in the data set. Thus, the information got from the 3D-QSAR analysis is relatively limited. Therefore, the molecular docking was used to further clarify the binding mode of the compounds and provide straightforward information for further structural optimization. Our homologous model of CACYP51 built from the crystal structure of MTCYP51 was used in the present docking study.[41] To evaluate the effectiveness of the Affinity

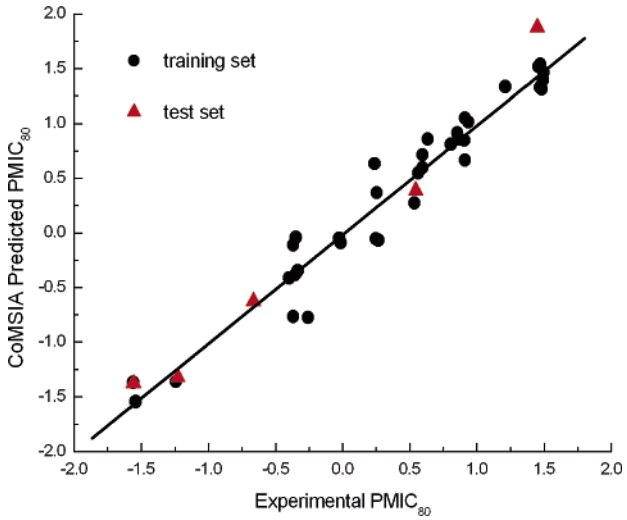

Figure 4. Experimental and calculated $pMIC_{80}$ for the CoMSIA analysis of the training set and test set.

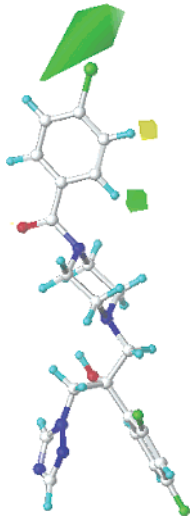

Figure 5. Contour plots of CoMFA steric field. Sterically favored areas (contribution level of 80%) are represented by green polyhedra, and sterically disfavored areas (contribution level of 20%) are represented by yellow polyhedra. Compound **9** is shown in ball-and-stick mode.

method[46] in the flexible docking of azole antifungal agents, the crystal structure of MTCYP51 in complex with fluconazole (PDB entry 1EA1) was chosen as a test case.[23] Using the flexible ligand docking procedure in the Affinity module within the InsightII software package, the observed crystallographic conformation can be reproduced with the RMSD value of 1.981 Å, indicating that this docking method can be used as a powerful tool to clarify the binding mode of the azole antifungal agents. The calculated interaction energies and LUDI scores[47,48] of each compound in the data set and fluconazole are given in Table 3. The calculated interaction energies of the compounds in the data set correlated well with the experimentally determined antifungal activity ($r^2 = 0.808$), indicating the interaction energy may be a useful parameter in optimizing the azole antifungal compounds.

The docked conformation of fluconazole into the active site of CACYP51 was similar to the bioactive conformation of fluconazole into the crystal complex of MTCYP51 (Figure 8), with the RMSD value of 0.4192 Å. The binding mode of fluconazole with CACYP51 was similar to that of our previous studies.[17] Fluconazole binds to the active site of CACYP51 through the formation of a coordination bond with iron of the

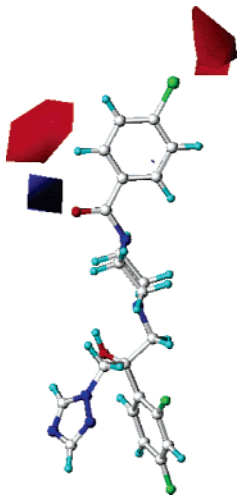

Figure 6. Contour plots of CoMFA electrostatic field. Positive charge favored areas (contribution level of 80%) are represented by red polyhedra, and positive charge disfavored areas (contribution level of 20%) are represented by blue polyhedra. Compound **9** is shown in ball-and-stick mode.

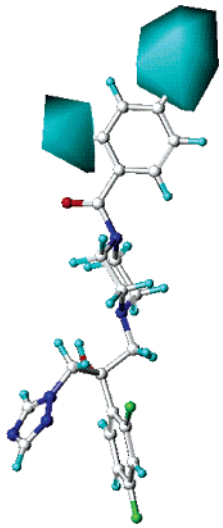

Figure 7. Contour plot of CoMSIA hydrophobic field. Cyan polyhedra indicates hydrophobic substituents favored regions with the contribution level of 80%, while magenta polyhedra indicating hydrophobic substituents disfavored regions is not shown with the contribution level of 20%. Compound **9** is shown in ball-and-stick mode.

heme group. The diflurophenyl group of fluconazole is located in the hydrophobic binding cleft lined with A114, F126, L139, M140, F145, I304, and M306, and the 17-side chain of the substrate was also found to be located in the same pocket.[25] Several residues lined with L121, T122, F228, T311, P375, L376, and M508 were observed to form indirect nonbonding interactions with another triazolyl ring attached to C3.

The development of novel triazole antifungal agents has been focused on the modification of the side chain attached to C3, and it is of great importance to understand the properties of the corresponding part in the active site of fungal CYP51. Therefore, the azoles in the data set can be used as probes to investigate the important residues in the active site of CACYP51 and to guide the design of more potent antifungal agents. Both *R* and *S* isomers of the compounds were considered in our docking studies, and they interacted with CACYP51 through a similar binding mode. However, *R* isomers showed lower interaction energy with CACYP51 than the *S* isomers, which indicated that the *R* isomers might have better antifungal activity than the *S*

Table 3. Calculated Interaction Energies (kcal/mol) for the Complexes of Triazole Antifungal Compounds with the Active Site of CACYP51, Ludi Scores, and Experimentally Determined Antifungal Activity (MIC_{80}, μmol/L)

compd	MIC_{80}	E_{vdw}	E_{elect}	E_{total}[a]	Ludi score 1[b]	Ludi score 2[c]
1	0.0339	−76.031	−6.011	−82.642	545	905
2	0.0350	−70.017	−7.884	−77.901	548	925
3	0.0324	−73.302	−4.734	−77.676	534	1017
4	0.0320	−70.050	−5.985	−76.035	560	1055
5	0.1372	−73.704	−4.7834	−78.487	521	941
6	2.4973	−70.636	4.792	−65.844	415	778
7	0.156	−68.549	−7.121	−75.670	465	972
8	0.1242	−80.832	−4.485	−85.317	610	1150
9	0.5412	−73.543	0.230	−73.313	468	793
10	2.2325	−64.854	−0.271	−65.125	468	786
11	2.1649	−56.585	−10.642	−67.227	550	809
12	1.0582	−66.842	−10.392	−77.234	416	785
13	16.9326	−69.903	3.297	−66.606	465	847
14	2.2651	−64.459	−2.447	−66.906	488	790
15	18.1208	−73.031	9.790	−63.241	452	908
16	0.2732	−73.342	−1.893	−75.235	533	900
17	36.2417	−64.745	−5.589	−70.334	447	790
18	36.1606	−64.392	11.829	−52.563	389	707
19	2.3394	−64.716	−3.155	−67.871	503	864
20	17.4871	−66.4795	7.675	−58.804	522	872
21	1.0339	−70.305	−7.351	−77.655	506	873
22	0.034	−85.038	3.989	−81.050	625	1024
23	0.0357	−72.062	−3.482	−75.544	489	965
24	0.1395	−73.894	−5.583	−79.477	520	946
25	0.5794	−72.371	−0.795	−73.166	474	868
26	0.2538	−73.373	−4.040	−77.413	543	961
27	2.3391	−76.951	−1.576	−78.527	528	914
28	0.2923	−78.007	5.196	−72.811	530	946
29	34.8986	−69.934	6.841	−63.093	368	695
30	0.1224	−78.975	−3.064	−81.859	528	963
31	0.1224	−72.547	−6.617	−78.714	539	929
32	0.2535	−69.422	−6.792	−76.213	409	750
33	0.0612	−80.855	−4.618	−85.423	507	957
34	0.5662	−80.565	4.362	−76.204	554	1061
35	0.5581	−70.449	−5.098	−75.547	516	944
36	0.2317	−74.093	−2.952	−77.045	540	911
37	0.1158	−74.624	−2.107	−76.731	561	969
38	0.0331	−82.108	−2.842	−84.950	596	1028
39	4.6354	−72.017	−1.346	−73.363	497	967
40	0.2850	−72.014	−3.366	−75.380	458	723
fluconazole	0.8162	−54.864	−3.199	−58.063	336	791

[a] $E_{total} = E_{vdw} + E_{elect}$. [b]The Ludi score 1 was calculated by the method in ref 10. [c]The Ludi score 2 was calculated by the method in ref 11. The difference between the LUDI score 1 and score 2 is that an additional term evaluating the contribution of binding of aromatic−aromatic interaction is added to LUDI score 2.

isomers. In the following discussion, all the docked conformations refer to the *R* configuration of the compounds. The docking results revealed that the general conformation of the compounds in the active site was similar to that of fluconazole. The distance between the N4 atom of triazolyl group and the iron of the heme group varies from 2.30 to ∼2.37 Å, which is suitable to form a coordination bond. The difluorophenyl group of the compounds is also located in the hydrophobic pocket lined with A114, F126, L139, M140, F145, I304, and M306. The hydrophobic interaction between them could stabilize the compounds in the active site. The hydroxyl group attached to C2 was important for the antifungal activity, but no interaction was observed between this hydroxyl group and the active site of CACYP51. In the crystal structure of MTCYP51 complexed with fluconazole, the active site is filled with water molecules and fluconazole interacts with at least three water molecules[23] which bridge the interactions with the active site. From the docking results, it is possible that the water molecules in the active site mediate the interaction between the hydroxyl group and the vicinal H310, which is a highly conserved residue in the CYP51 family and has been found to form a hydrogen bond with the 3-OH of the substrate in our previous studies.[25]

Crystal structures of MTCYP51 and other P450 proteins revealed that there were two putative substrate access channels (channel 1 and channel 2).[23] Channel 1 is parallel to the plane of the heme group and is formed by the bending the helix I away from the heme, which released the BC loop in an open conformation. Channel 2 is perpendicular to the plane of heme group and its entrance is surrounded by helix A′ and FG loop. Channel 1 is apparent in the crystal structure of MTCYP51 and P450 2C5, and channel 2 is based on the crystal structure of P450BM3. In our model of CACYP51, the ligand access channel shared similar topological features to that of MTCYP51, with BC loop having an open conformation and FG loop having a closed conformation.[25] Flexible docking results indicated that the piperazinyl side chains of the compounds had preferable orientation into channel 2, which is consistent with a recent docking result of posaconazole with CACYP51.[37] Moreover, the resulting binding model can well explain the structure−antifungal activity relationship of the compounds in the data set. The piperazinyl group of the side chain interacted with the surrounding hydrophobic residues such as A117, L376, and I379. The phenyl group of the side chain interacts with the phenol group of Y118 through the formation of $\pi-\pi$ face-to-edge interaction. This result is consistent with the CoMFA electrostatic contour map in that electron-rich (or electron-withdrawing) groups are favored in the ortho- and para-position of the phenyl group. Furthermore, a docking model of 1,4-

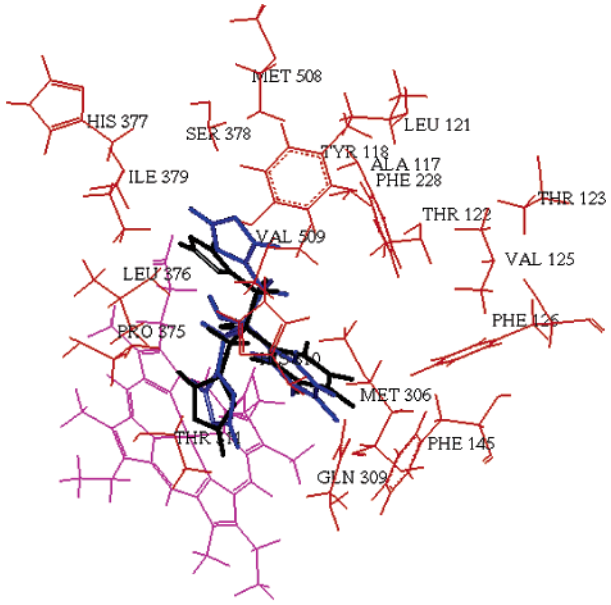

Figure 8. Docking of fluconazole into the active site of CACYP51 and residues within 6 Å from the ligand are shown. The docked conformation of fluconaole (blue) and its conformation in the crystal structure of MTCYP51 (black) are superimposed.

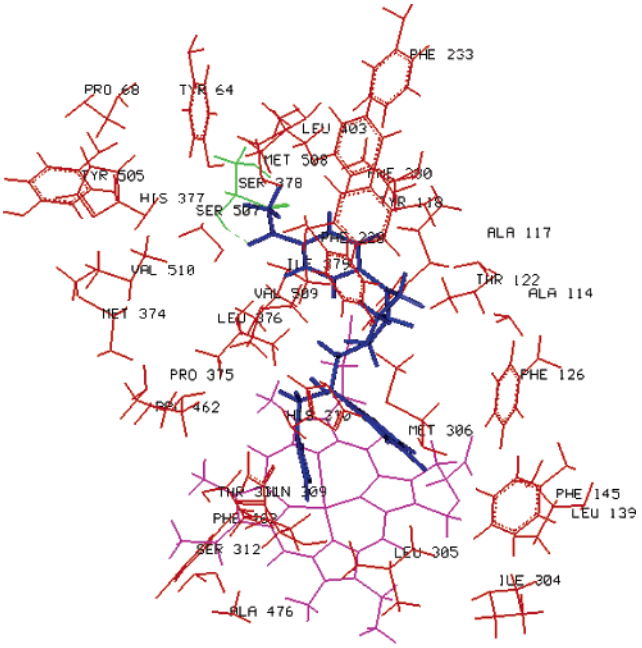

Figure 9. Docking of compound **2** into the active site of CACYP51 and the residues within 6 Å from the ligand are shown. The hydrogen bonds are indicated with dotted lines.

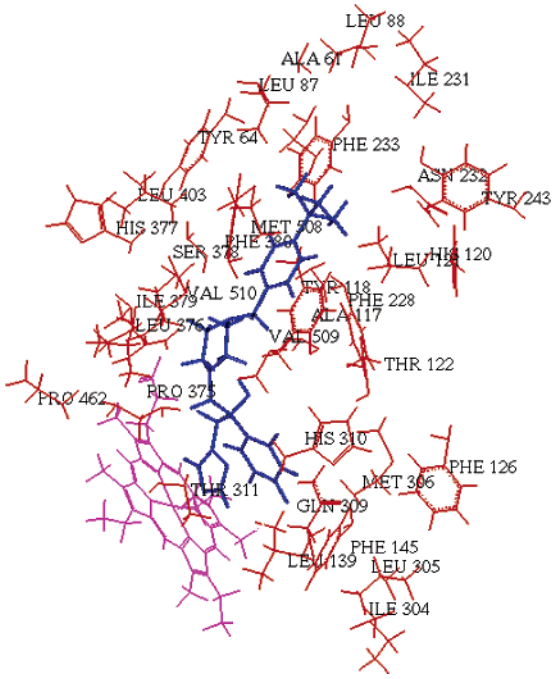

Figure 10. Docking of compound **22** into the active site of CACYP51 and the residues within 6 Å from the ligand are shown.

benzothiazine and 1,4-benzixazine imidazole derivatives with CACYP51 also found Y118 could form $\pi-\pi$ interaction with the inhibitors.[49] Y118 is a highly conserved residue through the CYP51 family, and site-directed mutagenesis of corresponding Y76 of MTCYP51 has revealed its importance in maintaining proper orientation of the heme.[50] Therefore, Y118 may be an important residue for the design of CACYP51 inhibitors.

Various substituent groups on the phenyl group could form different interactions with the active site of CACYP51, which resulted in the different antifungal activity. Docking results of compounds **1**, **2**, and **3** showed that all the three compounds could form a hydrogen bond with the side chain of S378 by the substitutions on the para-position of the phenyl group (Figure 9). In our previous studies, S378 was used as a hydrogen bond site to design *non*-azole inhibitors, and the results supported our hypothesis.[22] Therefore, we suggest that S378 is an important residue in the design of CACYP51 inhibitors. Compounds with steric and hydrophobic substitutions on the para-position of the phenyl (e.g. compound **5** and **22**) also show excellent antifungal activity, which is attributed to the hydrophobic and van der Waals interactions with L121, F233, and M508. From the docking results, there remained a relatively large space near the para-position of the phenyl group, and this area is at the end of ligand access channel 2 (FG loop) lined with hydrophobic residues such as L87, L88, L121, P230, I231, F233, V234, and M508 (Figure 10). Therefore, the side chain of azoles in the data set could be extended to form stronger hydrophobic and van der Waals interactions with the active site of CACYP51. Compared to compounds **23**, **25**, and **26**, compounds **30**, **31**, and **33** show higher antifungal activity. It is because the addition of a halogen on the phenyl can form a stronger hydrophobic interaction with the active site of CACYP51. When the benzyl groups of compounds **22**−**40** are changed into benzoyl groups (compounds **9**−**21**), their antifungal activity is decreased dramatically. From the docking results, we found that a hydrogen bond was formed between the carbonyl group and the backbone of F380, which resulted in the moving of phenyl group away from Y118 and the $\pi-\pi$ interaction between them was lost. Correspondingly, the interaction energies, especially LUDI score 2,[48] were decreased.

Design, Synthesis, and Antifungal Activities of Novel Azoles Based on 3D-QSAR and Docking. 3D-QSAR and molecular docking are two complementary methods, and the combination of them is especially useful when the high-resolution ligand−receptor structure is unavailable. In the present study, the crystal structure of CACYP51 has not been solved until now, and the combination of 3D-QSAR and molecular docking studies can provide precise information to guide the drug design. Based on the findings from 3D-QSAR and docking studies, a pharmacophore model was generated to

Chart 2

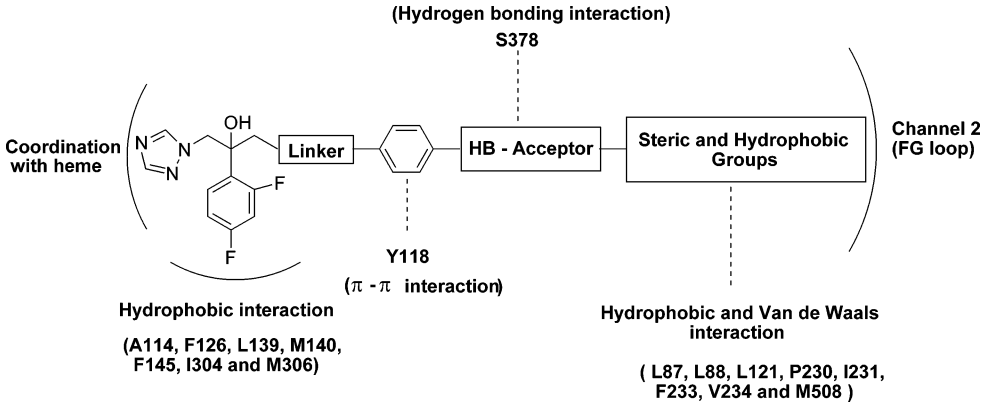

Chart 3

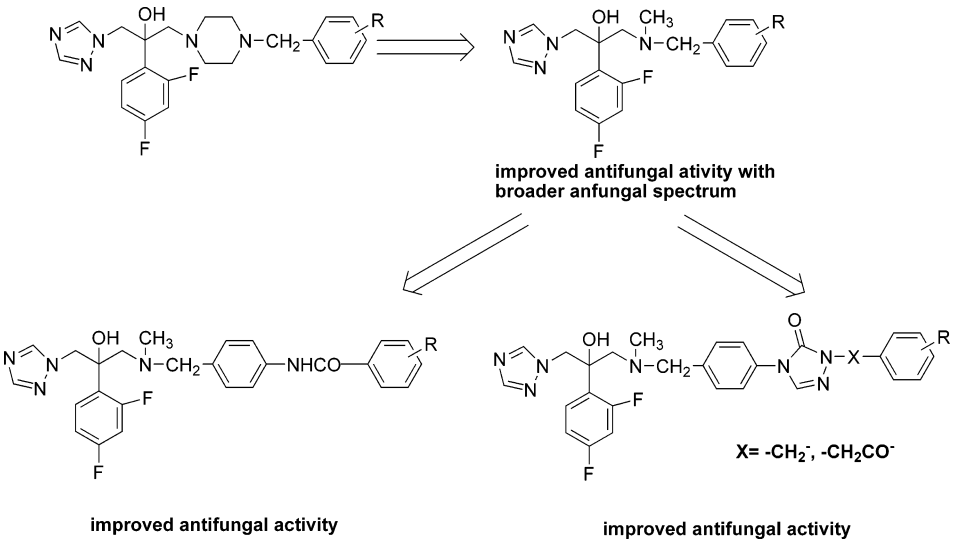

guide the further rational optimization of the compounds in data set (Chart 2). In this model, we mainly focused on the optimization of the side chain attached to C3. First, a linker is necessary to restrict the side chain in proper conformation and adjust the physicochemical properties of the whole molecule. Second, a phenyl group is a suitable attachment to the linker because it can form a $\pi-\pi$ interaction with Y118. Third, a hydrogen bond acceptor is favored at the para-position of the phenyl, which could form hydrogen bonding interaction with S378. Last, a steric and hydrophobic group is necessary because it could form hydrophobic and van der Waals interactions with the corresponding residues in the ligand access channel 2 (FG Loop). Therefore, a three-step optimization of the azole antifungal agents was performed on the basis of the present pharmacophore model (Chart 3). During this process, both predicted activities from 3D-QSAR and interaction energies from molecular docking were considered in determining the compounds for synthesis.

First, we attempted to change the linker between the C3 and the phenyl group. Docking results revealed that the piperazinyl group was not the best choice and a smaller linker would be more favorable for the $\pi-\pi$ interaction of the phenyl group with Y118. After testing various linkers based on 3D-QSAR predictive values and the interaction energy with CACYP51, we chose the $-N-CH_3$ group for synthesis because the improved flexibility of the molecule allows the phenyl group to more easily lock its proper position, and the methyl group could form additional van der Waals interactions with the surrounding A117, L376, and I379. A total of 13 compounds with benzylamine side chains (compounds **45**−**57**) were synthesized. In vitro antifungal activity assay indicated that their antifungal activities were higher than those of corresponding compounds with piperazinyl groups (Tables 4 and 5). Moreover, these compounds showed a broader antifungal spectrum with good activity against both systemic pathogenic fungi (e.g. *C. albicans*, *Cryptococcus neoformans*, *A. fumigatus*) and dermatophytes, (e.g. *Trichophyton rubrum* and *Trichophyton mentagrophytes*). Especially, compound **53** showed excellent activity against most of the tested pathogenic fungi, and it was a good candidate for developing novel azole antifungal agents with broad spectrum.

Second, we extended the side chain of the benzylamine analogues on the basis of the pharmacophore model. Amide was selected as the hydrogen bond acceptor to be attached to the phenyl group, which was designed to form a hydrogen bond with S378. Then, we chose substituted phenyl groups as steric and hydrophobic groups to attach the amide group in order to form additional hydrophobic and van der Waals interaction with the residues in the ligand access channel 2 (FG loop). A total of 10 amide-benzylamine compounds (compounds **58**−**67**) were synthesized and tested for in vitro antifungal activity. Most of them showed improved antifungal activity in comparison with the benzylamine compounds (Table 6), which was attributed to the additional hydrogen bonding and hydrophobic interaction with the target enzyme. Most of the compounds showed better activity against *C. albicans* and *Crypt. neoformans* than flu-

Table 4. Antifungal in Vitro Activities of the Benzylamine Compounds (MIC_{80}, $\mu g \cdot mL^{-1}$)[a]

compd	*C. alb.*	*C. par.*	*C. tro.*	*C. neo.*	*A. fum.*	*F. ped.*	*T. rub.*	*S. sch.*
45	0.032	≤0.125	≤0.125	0.25	0.5	0.25	≤0.125	32
46	2	2	0.25	0.25	4	1	0.25	64
47	0.032	0.25	≤0.125	≤0.125	4	0.25	1	64
48	0.032	≤0.125	≤0.125	≤0.125	4	2	0.5	64
49	0.5	≤0.125	0.25	0.5	8	1	32	64
50	0.032	≤0.125	≤0.125	≤0.125	0.5	≤0.125	0.25	64
51	0.032	0.25	≤0.125	≤0.125	8	0.25	≤0.125	32
52	1	1	≤0.125	≤0.125	8	≤0.125	≤0.125	64
53	0.032	0.25	≤0.125	≤0.125	≤0.125	≤0.125	≤0.125	16
54	0.016	1	≤0.125	≤0.125	4	≤0.125	≤0.125	32
55	0.031	2	1	0.25	8	0.125	0.5	64
56	0.032	4	0.25	0.5	64	1	8	64
57	0.0625	2	0.5	8	64	4	16	64
Flu	0.25	0.5	0.5	16	32	64	8	>64
Ket	0.0625	≤0.125	≤0.125	≤0.125	1	≤0.125	≤0.125	0.5
Ter	16	16	32	4	0.25	≤0.125	≤0.125	2

[a] Abbreviations: *C. alb.*, *Candida albicans*; *C. par.*, *Candida paropsilosis*; *C. tro.*, *Candida tropicalis*; *C. neo.*, *Cryptococcus neoformans*; *A. fum.*, *Aspergillus fumigatus*; *F. ped.*, *Fonsecaea pedrosoi*; *T. rub.*, *Trichophyton rubrum*; *S. sch.*, *Sporothrix schenckii*; Flu, fluconazole; Ter, terbinafine; Ket, ketoconazole.

Table 5. Antifungal in Vitro Activities of Benzylamine Compounds against Dermatophytes (MIC_{80}, $\mu g \cdot mL^{-1}$)[a]

compd	*M. gyp.*	*T. vio.*	*M. lan.*	*T. men.*	*E. flo.*
45	0.5	0.25	<0.0625	<0.0625	<0.0625
47	32	2	4	0.125	<0.0625
48	32	4	8	0.5	<0.0625
49	8	2	0.5	<0.0625	<0.0625
50	32	2	1	<0.0625	<0.0625
51	4	0.5	0.25	<0.0625	<0.0625
52	0.125	<0.0625	<0.0625	<0.0625	<0.0625
53	<0.0625	<0.0625	<0.0625	<0.0625	<0.0625
54	16	4	8	<0.0625	<0.0625
Flu	8	32	>32	>32	>32
Ket	<0.0625	0.25	<0.0625	<0.0625	<0.0625
Ter	<0.0625	4	32	>32	>32

[a] Abbreviations: *M. gyp.*, *Microsporum gypseum*; *T. vio.*, *Trichophyton violaceum*; *M. lan*, *Microsporum lanosum*; *T. men.*, *Trichophyton mentagrophytes*; *E. flo.*, *Epidermophyton floccosum.*

Table 6. Antifungal in Vitro Activities of the Amide-Benzylamine Compounds (MIC_{80}, $\mu g \cdot mL^{-1}$)[a]

compd	*C. alb.*	*C. par.*	*C. tro.*	*C. neo.*	*A. fum.*	*F. ped.*	*T. rub.*	*M. lan.*
58	0.031	0.0625	0.125	1	32	1	0.5	4
59	0.016	0.031	0.016	0.25	32	≤0.125	≤0.125	8
60	0.0625	0.125	0.5	0.5	>64	0.25	0.5	4
61	0.016	0.031	0.016	0.5	32	0.25	≤0.125	2
62	0.031	0.0625	1	1	16	0.5	≤0.125	0.25
63	0.016	0.125	0.5	0.0625	16	≤0.125	0.5	0.5
64	16	16	4	0.5	64	0.5	0.25	8
65	0.0625	0.5	0.25	≤0.031	>64	≤0.125	≤0.125	≤0.125
66	0.0625	0.25	0.5	2	32	2	4	2
67	0.008	0.016	0.016	0.125	16	≤0.125	≤0.125	0.25
Flu	0.25	0.5	1	4	>64	32	64	64
Ket	0.0625	0.0625	0.0625	0.5	2	0.25	4	4
Itz	0.125	0.25	0.125	2	1	0.5	1	1
Ter	2	>16	>16	1	≤0.125	≤0.125	≤0.125	≤0.125

[a] Abbreviations: *C. alb.*, *Candida albicans*; *C. par.*, *Candida paropsilosis*; *C. tro.*, *Candida tropicalis*; *C. neo.*, *Cryptococcus neoformans*; *A. fum.*, *Aspergillus fumigatus*; *F. ped.*, *Fonsecaea pedrosoi*; *T. rub.*, *Trichophyton rubrum*; *M. lan*, *Microsporum lanosum*; Flu, fluconazole; Ket, ketoconazole; Itz, itraconazole; Ter, terbinafine.

conazole, itraconazole, and ketoconazole, with their MIC_{80} values in the range of 0.125 μg/mL to 0.008 μg/mL. Compounds **59**, **61**, **63**, and **67** exhibited strong in vitro antifungal activity with broad antifungal spectrum, which was worthy of further evaluation.

Third, we chose the triazolone group to replace the amide group as a hydrogen bond acceptor because triazolone group can not only form a hydrogen bond with S378 but also can adjust the phsicochemical properties of the molecules and improve the water solubility. Various substituted benzyl groups and substituted 2-oxophenethyl groups were attached to the triazolone group to form hydrophobic interaction with the residues in the ligand access channel 2 (FG loop). These compounds showed better 3D-QSAR predictive activities and interaction energies with CACYP51 than the corresponding benzylamine or amide-benzylamine compounds. Therefore, we synthesized 34 new azoles with triazolone-benzylamine side chains (compounds **76**−**109**). In vitro antifungal assay revealed that their antifungal activities were improved again (Table 7), and most of them showed the best antifungal activities among the synthesized azoles with their MIC_{80} values against *C. albicans* in the range of 0.004 μg/mL to 0.001 μg/mL. Compound **94** was the most active among the designed compounds with MIC_{80} value of 0.001 μg/mL against *C. albicans*, and further pharmacological and toxicological evaluation is in progress.

Table 7. Antifungal in Vitro Activities of the Triazolone-Benzylamine Compounds (MIC_{80}, $\mu g \cdot mL^{-1}$)[a]

compd	*C. alb.*	*C. par.*	*C. tro.*	*C. neo.*	*A. fum.*	*F. ped.*	*T. rub.*	*S. sch.*
76	0.002	0.125	0.5	1	32	0.25	1	64
77	0.0625	0.25	0.0625	16	64	4	16	64
78	0.004	4	1	4	64	1	8	32
79	0.031	4	1	2	8	0.25	0.5	32
80	0.031	2	0.0625	1	32	0.0625	1	64
81	0.004	0.06	0.125	1	32	0.5	4	32
82	0.016	4	0.5	0.5	8	0.125	0.5	32
83	0.008	0.008	0.25	0.5	8	0.25	0.5	64
84	0.002	0.008	0.0625	0.008	2	0.125	0.25	4
85	0.002	0.008	0.0625	0.5	4	0.125	0.5	64
86	0.031	0.016	1	64	64	0.5	16	64
87	0.031	0.031	1	0.25	2	0.0625	0.25	64
88	0.002	0.008	0.0625	0.25	2	0.0625	0.25	64
89	0.002	0.008	0.0625	0.008	8	0.0625	0.25	64
90	0.004	0.008	0.125	1	16	1.25	0.5	64
91	0.002	0.008	0.0625	0.125	4	0.125	0.5	64
92	0.004	0.008	0.125	0.125	16	0.25	1	64
93	0.002	0.008	0.25	0.5	32	0.25	2	16
94	0.001	0.008	0.0625	0.25	8	0.0625	0.5	16
95	0.002	0.008	0.0625	0.125	16	0.125	0.5	64
96	0.002	0.008	0.03125	0.016	8	0.125	0.25	32
97	0.031	1	0.125	16	64	4	32	64
98	0.0625	2	0.5	32	64	2	64	64
99	0.002	0.008	0.03125	0.125	16	0.125	1	64
100	0.002	0.125	0.0625	0.5	8	0.0625	0.5	64
101	0.25	2	0.5	16	64	8	32	64
102	0.004	0.03	0.0625	2	64	0.25	4	64
103	0.004	0.06	0.0625	1	64	0.0625	2	64
104	0.002	1	0.0625	0.25	16	0.0625	0.25	64
105	0.016	0.03	0.125	8	32	1	4	64
106	0.004	0.06	0.125	1	32	0.125	1	64
107	0.016	0.008	0.0625	8	64	1	8	64
108	0.125	0.5	0.0625	64	32	1	64	64
109	0.008	0.016	0.0625	8	64	2	4	64
Flu	0.25	0.5	0.5	16	32	64	8	>64
Ket	0.0625	0.031	0.0625	0.031	1	0.0625	0.0625	0.5
Ter	16	16	32	4	0.25	≤0.125	≤0.125	2

[a] Abbreviations: *C. alb.*, *Candida albicans*; *C. par.*, *Candida paropsilosis*; *C. tro.*, *Candida tropicalis*; *C. neo.*, *Cryptococcus neoformans*; *A. fum.*, *Aspergillus fumigatus*; *F. ped.*, *Fonsecaea pedrosoi*; *T. rub.*, *Trichophyton rubrum*; *S. sch.*, *Sporothrix schenckii*; Flu, fluconazole; Ter, terbinafine; Ket, ketoconazole.

Conclusion

In response to the emergent need for novel azole antifungal agents with improved activity and broader antifungal spectrum, we sought to understand the necessary structural features for antifungal activities and then to design new potent inhibitors by use of a structure-based strategy. In the present study, we have established predictive CoMFA and CoMSIA 3D-QSAR models for a set of newly synthesized triazole antifungal compounds from our laboratory. The best derived CoMFA and CoMSIA models showed a predictive q^2 value of 0.718 and 0.655, and the activities of compounds in the data set were predicted with high accuracy. Moreover, molecular docking was used to clarify the binding mode of the azoles in the data set. The side chain attached to C3 had a major impact on antifungal activity, which was found to be located in the ligand access channel 2 in the active site of CACYP51. Y118 and S378 could form specific $\pi-\pi$ interactions and hydrogen bonding interactions with the inhibitors, which were very important for drug design. The results obtained from 3D-QSAR and molecular docking yielded reliable clues on how to further optimize the azoles in the data set. Therefore, a receptor-based pharmacophore model for the rational optimization of azole antifungal agents was established. A three-step optimization process was performed based on this model with 3D-QSAR predictive values and interaction energies as criteria to select compounds for synthesis. A total of 57 novel azoles with three different types of side chains were designed and synthesized, and their antifungal activities were greatly improved, which confirmed the powerfulness of the combination of 3D-QSAR and molecular docking in the optimization of azole antifungal agents. Several compounds (such as **53**, **67**, and **94**) showed strong in vitro antifungal activity against most of the tested pathogenic fungi. However, the in vitro antifungal activity of the azoles does not always correlate well with their in vivo efficiency because many azoles are very hydrophobic and their bioavailability is relatively low. Thus, only when our synthesized azoles have good pharmacokinetic and toxicological profiles can they be developed into novel triazole antifungal agents. Further pharmacological and toxicological evaluation of these promising compounds is in progress. Our study demonstrates the efficiency of 3D-QSAR and molecular docking not only for understanding the molecular basis of drug−enzyme interaction but also for the discovery and optimization of the lead compounds.

Experimental Section

Chemistry. General Methods. Melting points were measured on an electrically heated XT4A instrument and are uncorrected. Infrared spectra (IR) were recorded on a Brucker Vector II instrument. Mass spectra (MS) were measured on a Micromass Qtof-Micro LC-MS instrument. Nuclear magnetic resonance (NMR) spectra were recorded on a Bruker 500 spectrometer with TMS as an internal standard and $CDCl_3$ as solvent. Elemental analyses were performed with a MOD-1106 instrument and were consistent with theoretical values within ±0.4%. Silica gel thin-layer chromatography was performed on precoated plates GF254 (Qindao Haiyang Chemical, China). Silica gel column chromatography was performed

with Silica gel 60 G (Qindao Haiyang Chemical, China). Commercial solvents were used without any pretreatment.

1-(1*H*-1,2,4-triazole-1-yl)-2-(2,4-difluorophenyl)-3-[*N*-methyl-*N*-(3-chlorobenzyl)-amino]-2-propanol (45). The mixture of epoxide **44** (3.3 g, 0.01 mol), MeOH (20 mL), NaOH (0.40 g, 0.01 mol), and 3-chloro-*N*-methyl-benzylamine (1.90 g, 0.012 mol) was stirred under the refluxing condition for 8 h. The solvent was evaporated under reduced pressure. The residue was triturated with H_2O (50 mL) and extracted with ethyl acetate (100 mL × 3). The combined organic layers were washed with H_2O (100 mL × 3) and brine (100 mL × 3), dried over anhydrous $MgSO_4$, and filtrated, and the solvent was evaporated under reduced pressure. The residue was purified by silica gel column chromatography (EtOAc:hexane 1:1, v/ v) to give **45** (2.67 g, 67.9%) as a white solid: mp 82−83 °C. IR (film): ν (cm^{-1}) = 3106, 1615, 1518, 1503. ^1H NMR ($CDCl_3$): δ 2.04 (s, 3H), 2.81 (d, J = 13.2 Hz, 1H), 3.07 (d, J = 13.2 Hz, 1H), 3.40 (d−d, J_1 = 13.2 Hz, J_2 = 38.8 Hz, 2H), 4.47 (d−d, J_1 = 14.4 Hz, J_2 = 28.4 Hz, 2H), 6.74∼7.60 (m, 7H), 7.74 (s, 1H), 8.06 (s, 1H). MS (ESI) *m*/*z*: 393 (M + 1). Anal. ($C_{19}H_{19}ClF_2N_4O$) C, H, N.

The synthetic methods for the following compounds **46**−**57** were similar to the synthesis of compound **45**.

***N*-[4-({[2-(2,4-Difluoro-phenyl)-2-hydroxy-3-[1,2,4]triazol-1-yl-propyl]-methyl-amino}-methyl)-phenyl]-benzamide (58).** A solution of benzoyl chloride (0.14 g, 0.001 mol) in 1,4-dioxane (10 mL) was added dropwise to a stirred mixture of compound **57** (0.37 g, 0.001 mol) and triethylamine (1.0 mL) in dioxane (15 mL) at 0 °C under nitrogen flow. The mixture was stirred at room temperature for 5 h, and the solvent was evaporated under reduced pressure. The residue was purified by silica gel column chromatography (CH_2Cl_2:MeOH 95:5, v/v) to give **58** (0.42 g, 67.9%) as a white solid: mp 88−90 °C. IR (film): ν (cm^{-1}) = 3226, 3109, 1659, 1599, 1520, 1500, 1469. ^1H NMR ($CDCl_3$): δ 2.50 (s, 3H), 2.85 (d, J = 4.2 Hz, 1H), 3.16 (d, J = 4.7 Hz, 1H), 3.59 (d, J = 4.7 Hz, 1H), 3.85 (d, J = 4.7 Hz, 1H), 4.55 (d−d, J_1 = 14.4 Hz, J_2 = 20.0 Hz, 2H), 7.08∼8.90 (m, 14H), 10.30 (s, 1H). MS (ESI) *m*/*z*: 478 (M + 1). Anal. ($C_{26}H_{25}F_2N_5O_2$) C, H, N.

The synthetic methods for the following compounds **59**−**67** were similar to the synthesis of compound **58**.

{4-[(*tert*-Butoxycarbonyl-methyl-amino)-methyl]-phenyl}-carbamic Acid Phenyl Ester (71). Phenyl chloroformate (17.2 g, 0.11 mol) was added dropwise to a stirred mixture of compound **70** (23.6 g, 0.1 mol), pyridine (8.5 g, 0.11 mol), and EtOAC (200 mL) at 0 °C. The mixture was stirred for 3 h at room temperature, then washed with water (200 mL × 3), dried over anhydrous $MgSO_4$, and filtrated. The solvent was evaporated under reduced pressure, and the deposited crystals were collected and washed with hexane to give **70** (34.8 g, 97.7%) as a white solid: mp 109−110 °C. ^1H NMR ($CDCl_3$): 1.48 (s, 9H), 2.82 (s, 3H), 4.39 (s, 2H), 7.00 (br, 1H), 7.18∼7.42 (m, 9H). MS (ESI) *m*/*z*: 357 (M + 1). Anal. ($C_{20}H_{24}N_2O_4$) C, H, N.

4-(*N*-methyl-*N*-Boc-aminomethyl)phenylsemicarbazide (72). A mixture of compound **71** (35.6 g, 0.1 mol), hydrazine hydrate (10 mL), and dimethoxyethane (150 mL) was stirred for 24 h. The solvent was evaporated under reduced pressure, and the residue was washed with EtOAc to give **72** as a white solid. ^1H NMR ($CDCl_3$): 1.48 (s, 9H), 2.81 (s, 3H), 3.84 (br, 2H), 4.36 (s, 2H), 6.76 (br, 1H), 7.16∼7.42 (m, 4H), 8.21 (s, 1H). MS (ESI) *m*/*z*: 295 (M + 1). Anal. ($C_{14}H_{22}N_4O_3$) C, H, N.

Methyl-[4-(5-oxo-1,5-dihydro-[1,2,4]triazol-4-yl)-benzyl]-carbamic Acid *tert*-Butyl Ester (73). A mixture of compound **72** (15.0 g, 0.05 mol), formamidine acetate (22.0 g, 0.2 mol), and DMF (250 mL) was stirred at room temperature for 30 min. AcOH (14.3 mL) was added, and the resulting mixture was heated for 6 h at 80 °C. The solvent was evaporated under reduced pressure, and the residue was poured onto the ice water. After filtration, the residue was recrystallized from EtOAC−hexane to give **73** (12.5 g, 82.2%) as a pale yellow solid. ^1H NMR ($CDCl_3$): 1.42 (s, 9H), 2.74 (s, 3H), 4.40 (s, 2H), 7.33∼7.67 (m, 4H), 8.31 (s, 1H), 11.80 (br, 1H). MS (ESI) *m*/*z*: 305 (M + 1). Anal. ($C_{15}H_{20}N_4O_3$) C, H, N.

Methyl-{4-[5-oxo-1-(4-trifluoromethyl-benzyl)-1,5-dihydro-[1,2,4]triazol-4-yl]-benzyl}-carbamic Acid *tert*-Butyl Ester (74). A mixture of compound **73** (1.5 g, 0.005 mol), 4-trifluoromethyl-benzyl chloride (2.9 g, 0.015 mol), and potassium carbonate (1.4 g, 0.01 mol) in DMF (15 mL) was heated at 80 °C for 18 h. The solvent was removed under reduced pressure. The residue was diluted with H_2O (50 mL) and extracted with ethyl acetate (50 mL × 3). The combined organic layers were washed with H_2O (100 mL × 3) and brine (100 mL × 3), dried over anhydrous $MgSO_4$, and filtrated, and the solvent was evaporated under reduced pressure. The resulting product was purified by silica gel column chromatography gradient elution, EtOAc/hexane 1/4 toward 1/1 to give **74** (1.80 g, 78.3%) as a white solid. ^1H NMR ($CDCl_3$): 1.42 (s, 9H), 2.78 (s, 3H), 4.41 (s, 2H), 5.07 (s, 2H), 7.35∼7.74 (m, 8H), 8.48 (s, 1H). MS (ESI) *m*/*z*: 463 (M + 1). Anal. ($C_{23}H_{25}F_3N_4O_3$) C, H, N.

4-(4-Methylaminomethyl-phenyl)-2-(4-trifluoromethyl-benzyl)-2,4-dihydro-[1,2,4]triazol-3-one (75). To a solution of compound **74** (1.8 g, 0.004mol) in EtOAc (25 mL) was added 20 mL of 10% HCl. The resulting mixture was stirred at room temperature for 24 h. The solvent was evaporated under reduced pressure. The residue was diluted with water (50 mL), basified with K_2CO_3, and extracted with $CHCl_3$ (50 mL × 3). The combined extract was washed with water (50 mL × 3) and brine (50 mL×3), dried over anhydrous $MgSO_4$, and filtrated, and the solvent was evaporated under reduced pressure to give compound **74** as a white solid. ^1H NMR ($CDCl_3$): 2.50 (s, 3H), 4.10 (s, 2H), 5.08 (s, 2H), 7.53∼7.80 (m, 8H), 8.55 (s, 1H). MS (ESI) *m*/*z*: 363 (M + 1). Anal. ($C_{18}H_{17}F_3N_4O$) C, H, N.

4-[4-({[2-(2,4-Difluoro-phenyl)-2-hydroxy-3-[1,2,4]triazol-1-yl-propyl]-methyl-amino}-methyl)-phenyl]-2-(4-methyl-benzyl)-2,4-dihydro-[1,2,4]triazol-3-one (76). The mixture of epoxide **44** (1.1 g, 0.0033 mol), EtOH (20 mL), triethylamine (2 mL), and 4-(4-methylaminomethyl-phenyl)-2-(4-methyl-benzyl)-2,4-dihydro-[1,2,4]-triazol-3 -one (1.0 g, 0.0033 mol) was stirred under refluxed for 8 h. The solvent was evaporated under reduced pressure. The residue was diluted with H_2O (50 mL) and extracted with ethyl acetate (50 mL × 3). The combined organic layers were washed with H_2O (100 mL × 3) and brine (100 mL × 3), dried over anhydrous $MgSO_4$, and filtrated, and the solvent was evaporated under reduced pressure. The residue was purified by silica gel column chromatography (CH_2Cl_2:MeOH 95:5, v/v) to give **76** (1.3 g, 74.1%) as a white solid: mp 80−82 °C. IR (film): ν (cm^{-1}) = 3413, 3126, 3054, 1710, 1615, 1554, 1500. ^1H NMR ($CDCl_3$): δ 1.24 (s, 3H), 2.03 (s, 3H), 2.40 (d, 2H), 3.72 (d−d, J_1 = 7.0 Hz, J_2 = 14.0 Hz, 2H), 4.47 (d−d, J_1 = 14.2 Hz, J_2 = 33.7 Hz, 2H), 5.00 (d, 2H), 6.80∼7.76 (m, 13H), 8.06 (s, 1H). MS (ESI) *m*/*z*: 547 (M + 1). Anal. ($C_{29}H_{29}F_2N_7O_2$) C, H, N.

The synthetic methods for the following compounds **77**−**109** were similar to the synthesis of compound **76**.

Computational Details. General Method. The crystallographic coordinates of MTCYP51 in complex with fluconazole (0.22 Å resolution, R_{cryst} = 0.204) were obtained from the Brookheaven Protein Databank as entries 1EA1. The 3D model of CYP51 from *C. albicans* was constructed in our previous studies.[25] All calculations were performed with the commercially available SYBYL6.9[51] software package and InsightII 2000[52] software package. All calculations were performed on an Origin 300 server.

Data Sets. A total of 40 azole antifungal compounds from our laboratory were used as a data set in the 3D-QSAR and docking analysis. In the CoMFA and CoMSIA study, five compounds (labeled with asterisks in Figure 1) were randomly selected as a test set, which represented a range of antifungal activity similar to that of a training set and was used to evaluate the predictive power of the resulting models. The biological activity of each compound was expressed as minimal inhibitory concentrations (MIC_{80}) against *C. albicans*, and −log(MIC_{80}) was used for the 3D-QSAR analysis.

Molecular Modeling and Alignment. The 3D structures of all compounds in the training set and test set were built from the SYBYL fragment library. Energy minimization was performed using the Tripos force field, Powell optimization method, and

MAXIMIN2 minimizer with a convergence criterion 0.001 kcal/mol·Å. Charges were calculated by the Gasteiger−Hückel method. The docked conformation of each compound in the active site of CACYP51 was used as pharmacophoric conformation for the 3D-QSAR studies. Compound **3**, one of the most active compounds, was used as the alignment template. The reference atoms used for alignment were three identified pharmacophoric points: N4 of the azole ring, the centroid of the phenyl ring, and the oxygen attached to C2.

CoMFA and CoMSIA Setup. The CoMFA descriptors, steric (Lennard-Jones 6-12 potential) and electrostatic (Coulombic potential) field energies, were calculated by the following parameters: an sp3 carbon probe atom with +1 charge and a van der Waals radius of 1.52 Å, and energy cutoff of 30 kcal/mol. CoMSIA similarity indices descriptors (steric, electrostatic, hydrophobic, H-bond donor, and H-bond acceptor fields) were calculated using a C1+ probe atom with a radius of 1.0 Å placed at grid spacing of 2 Å. CoMSIA similarity indices (A_F) for a molecule j with atoms i at a grid point q are calculated by eq 1:

$$A_{F,K}^{q}(j) = -\sum \omega_{\text{probe}'k}\omega_{ik}\, e^{-\alpha r_{iq}^2} \quad (1)$$

where k represents the following physicochemical properties: steric, electrostatic, hydrophobic, H-bond donor, and H-bond acceptor. A Gaussian type distance dependence was used between the grid point q and each atom i of the molecule. Here, steric indices are related to the third power of the atomic radii, electrostatic descriptors are derived from atomic partial charges, hydrophobic fields are derived from atom-based parameters, and H-bond donor and acceptor indices are obtained by a rule-based method based on experimental results. The attenuation factor (α) was set to the default value of 0.3.

The CoMFA and CoMSIA descriptors were used as independent variables, and $pMIC_{80}$ values were used as dependent variables in partial least squares (PLS)[53] regression analyses to derive 3D-QSAR models using the standard implementation in the SYBYL package. To obtain the optimum number of principle components, the leave-one-out (LOO) cross-validation[53] was utilized, which is used to be a measure of how good the model represents the data in the training set. The cross-validated coefficient, q^2, was calculated using eq 2:

$$q^2 = 1 - \frac{\sum (Y_{\text{predicted}} - Y_{\text{observed}})^2}{\sum (Y_{\text{observed}} - Y_{\text{mean}})^2} \quad (2)$$

where $Y_{\text{predicted}}$, Y_{observed}, and Y_{mean} are predicted, actual (observed), and mean values of the target property ($pMIC_{80}$), respectively. Conventional correlation coefficient r^2 and its standard error (s) were also computed for the final PLS models. To graphically interpret the 3D-QSAR results in terms of field contributions, isocontour maps were generated using the field type "stdev*coeff" and the contour levels were set to default values.

Docking Analysis. Fluconazole and the antifunal azoles in the data set were manually docked into the active site of CACYP51 on the basis of the binding mode of fluconazole with MTCYP51 and our previous docking studies.[17] First, the N4 atom of the azole ring was initially placed at 2.34 Å from the heme iron, and the distance was the same as that in the crystal structure of MTCYP51 in complex with fluconazole. Second, the difluorophenyl group was placed at the hydrophobic pocket lined with F126, L139, P145, I304, and M306. Third, the relatively reasonable positions of the azoles were obtained by monitoring the interaction energy between the ligands and CACYP51.

Then, the flexible ligand docking procedure in the Affinity module within InsightII was used to define the lowest energy position for the substrate using a Monte Carlo docking protocol. All the atoms within a defined radius (8 Å) of the substrate were allowed to move. The solvation grid supplied with the affinity Program was used. If the resulting substrate/enzyme system was within a predefined energy tolerance of the previous structure, the system was subjected to minimization. The resulting structure was accepted on the basis of energy check, which used the Metropolis criterion, and also a check of rms distance of the new structure versus the structure found so far. The final conformation was obtained through a simulation annealing procedure from 500 K to 300 K, and then 5000 rounds of energy minimization were performed to reach a convergence, where the resulting interaction energy values were used to define a rank order. Each energy-minimized final docking position of the compounds was evaluated using the interaction score function in the LUDI[54] module.

In Vitro Antifungal Activity Assay. In vitro antifungal activity was measured by means of the minimal inhibitory concentrations (MIC) using the serial dilution method in 96-well microtest plates. Test fungal strains were obtained from the ATCC or were clinical isolates. The MIC determination was performed according to the National Committee for Clinical Laboratory Standards (NCCLS) recommendations with RPMI 1640 (Sigma) buffered with 0.165 M MOPS (Sigma) as the test medium. The MIC value was defined as the lowest concentration of test compounds that resulted in a culture with turbidity less than or equal to 80% inhibition when compared with the growth of the control. Test compounds were dissolved in DMSO serially diluted in growth medium. The yeasts were incubated at 35 °C and the dermatophytes at 28 °C. Growth MIC was determined at 24 h for *Candida* species, at 72 h for *Crypt. neoformans*, and at 7 days for filamentous fungi.

Acknowledgment. We thank Professor Yuanyin Jiang of The Second Military Medical University for determining in vitro antifungal activities. This work was supported by the National Natural Science Foundation of China (Grant No. 30430750).

Supporting Information Available: IR, NMR, MS, and elemental analysis data for the compounds in this study. This material is available free of charge via the Internet at http://pubs.acs.org.

References

(1) Fridkin, S. K.; Jarvis, W. R. Epidemiology of nosocomial fungal infections. *Clin. Microbiol. Rev.* **1996**, *9*, 499−511.
(2) Latge, J. P. Aspergillus fumigatus and aspergillosis. *Clin. Microbiol. Rev.* **1999**, *12*, 310−350.
(3) Steenbergen, J. N.; Casadevall, A. Prevalence of Cryptococcus neoformans var. neoformans (Serotype D) and Cryptococcus neoformans var. grubii (Serotype A) isolates in New York City. *J. Clin. Microbiol.* **2000**, *38*, 1974−1976.
(4) Sheehan, D. J.; Hitchcock, C. A.; Sibley, C. M. Current and emerging azole antifungal agents. *Clin. Microbiol. Rev.* **1999**, *12*, 40−79.
(5) Gallis, H. A.; Drew, R. H.; Pickard, W. W. Amphotericin B: 30 years of clinical experience. *Rev. Infect. Dis.* **1990**, *12*, 308−329.
(6) Arikan, S.; Rex, J. H. Nystatin LF (Aronex/Abbott). *Curr. Opin. Invest. Drugs* **2001**, *2*, 488−495.
(7) Denning, D. W. Echinocandins: a new class of antifungal. *J. Antimicrob. Chemother.* **2002**, *49*, 889−891.
(8) Birnbaum, J. E. Pharmacology of the allylamines. *J. Am. Acad. Dermatol.* **1990**, *23*, 782−785.
(9) Cha, R.; Sobel, J. D. Fluconazole for the treatment of candidiasis: 15 years experience. *Expert. Rev. Anti-Infect. Ther.* **2004**, *2*, 357−366.
(10) Hoffman, H. L.; Ernst, E. J.; Klepser, M. E. Novel triazole antifungal agents. *Expert Opin. Invest. Drugs* **2000**, *9*, 593−605.
(11) Casalinuovo, I. A.; Di Francesco, P.; Garaci, E. Fluconazole resistance in *Candida albicans*: a review of mechanisms. *Eur. Rev. Med. Pharmacol. Sci.* **2004**, *8*, 69−77.
(12) Chandrasekar, P. H.; Manavathu, E. Voriconazole: A second-generation triazole. *Drugs Today (Barc.)* **2001**, *37*, 135−148.
(13) Herbrecht, R. Posaconazole: a potent, extended-spectrum triazole anti-fungal for the treatment of serious fungal infections. *Int. J. Clin. Pract.* **2004**, *58*, 612−624.
(14) Arikan, S.; Rex, J. H. Ravuconazole Eisai/Bristol-Myers Squibb. *Curr. Opin. Invest. Drugs* **2002**, *3*, 555−561.
(15) Aoyama, Y.; Yoshida, Y.; Sato, R. Yeast cytochrome P-450 catalyzing lanosterol 14α-demethylation. II. Lanosterol metabolism by purified P-450(14)DM and by intact microsomes. *J. Biol. Chem.* **1984**, *259*, 1661−1666.
(16) Lamb, D. C.; Kelly, D. E.; Venkateswarlu, K.; Manning, N. J.; Bligh, H. F.; Schunck, W. H.; Kelly, S. L. Generation of a complete, soluble, and catalytically active sterol 14α-demethylase-reductase complex. *Biochemistry* **1999**, *38*, 8733−8738.

(17) Ji, H.; Zhang, W.; Zhou, Y.; Zhang, M.; Zhu, J.; Song, Y.; Lu, J. A three-dimensional model of lanosterol 14α-demethylase of *Candida albicans* and its interaction with azole antifungals. *J. Med. Chem.* **2000**, *43*, 2493−2505.
(18) Ravichandran, K. G.; Boddupalli, S. S.; Hasermann, C. A.; Peterson, J. A.; Deisenhofer, J. Crystal structure of hemoprotein domain of P450BM-3, a prototype for microsomal P450's. *Science* **1993**, *261*, 731−736.
(19) Poulos, T. L.; Finzel, B. C.; Howard, A. J. High-resolution crystal structure of cytochrome P450cam. *J. Mol. Biol.* **1987**, *195*, 687−700.
(20) Hasemann, C. A.; Ravichandran, K. G.; Peterson, J. A.; Deisenhofer, J. Crystal structure and refinement of cytochrome P450terp at 2.3 A resolution. *J. Mol. Biol.* **1994**, *236*, 1169−1185.
(21) Cupp-Vickery, J. R.; Poulos, T. L. Structure of cytochrome P450eryF involved in erythromycin biosynthesis. *Nat. Struct. Biol.* **1995**, *2*, 144−153.
(22) Ji, H.; Zhang, W.; Zhang, M.; Kudo, M.; Aoyama, Y.; Yoshida, Y.; Sheng, C.; Song, Y.; Yang, S.; Zhou, Y.; Lu, J.; Zhu, J. Structure-based de novo design, synthesis, and biological evaluation of non-azole inhibitors specific for lanosterol 14α-demethylase of fungi. *J. Med. Chem.* **2003**, *46*, 474−485.
(23) Podust, L. M.; Poulos, T. L.; Waterman, M. R. Crystal structure of cytochrome P450 14α-sterol demethylase (CYP51) from *Mycobacterium tuberculosis* in complex with azole inhibitors. *Proc. Natl. Acad. Sci. U.S.A.* **2001**, *98*, 3068−3073.
(24) Podust, L. M.; Yermalitskaya, L. V.; Lepesheva, G. I.; Podust, V. N.; Dalmasso, E. A.; Waterman, M. R. Estriol bound and ligand-free structures of sterol 14α-demethylase. *Structure. (Camb.)* **2004**, *12*, 1937−1945.
(25) Sheng, C.; Zhang, W.; Zhang, M.; Song, Y.; Ji, H.; Zhu, J.; Yao, J.; Yu, J.; Yang, S.; Zhou, Y.; Zhu, J.; Lu, J. Homology modeling of lanosterol 14α-demethylase of *Candida albicans* and Aspergillus fumigatus and insights into the enzyme−substrate Interactions. *J. Biomol. Struct. Dyn.* **2004**, *22*, 91−99.
(26) Sheng, C. Q.; Zhu, J.; Zhang, W. N.; Song, Y. L.; Zhang, M.; Ji, H. T.; Yu, J. X.; Yao, J. Z.; Yang, S.; Miao, Z. Y. Synthesis and antifungal activity of novel triazole antifungal agents. *Yaoxue Xuebao* **2004**, *39*, 984−989.
(27) Sheng, C. Q.; Zhang, W. N.; Ji, H. T.; Song, Y. L.; Yang, S.; Zhou, Y. J.; Zhu, J.; Lu, J. G. Synthesis and antifungal activity of 1-(1,2,4-triazolyl-1H-1-yl)-2-(2,4-diflurophenyl)-3-(4-substituted benzyl-1-piperazinyl)-2-propanols. *Yaoxue Xuebao* **2003**, *38*, 665−670.
(28) Fratev, F.; Benfenati, E. 3D-QSAR and molecular mechanics study for the differences in the azole activity against yeastlike and filamentous fungi and their relation to P450DM inhibition. 1. 3-substituted-4(3H)-quinazolinones. *J. Chem. Inf. Model.* **2005**, *45*, 634−644.
(29) Kidwai, M.; Venkatarmanan, R.; Rastogi, S.; Sapra, P. Discovery and development of antifungal compounds. *Curr. Med. Chem. − Anti-Infect. Agents* **2003**, *2*, 27−71.
(30) Liu, J.; Pan, D.; Tseng, Y.; Hopfinger, A. J. 4D-QSAR analysis of a series of antifungal p450 inhibitors and 3D-pharmacophore comparisons as a function of alignment. *J. Chem. Inf. Comput. Sci.* **2003**, *43*, 2170−2179.
(31) Tafi, A.; Anastassopoulou, J.; Theophanides, T.; Botta, M.; Corelli, F.; Massa, S.; Artico, M.; Costi, R.; Di Santo, R.; Ragno, R. Molecular modeling of azole antifungal agents active against *Candida albicans*. 1. A comparative molecular field analysis study. *J. Med. Chem.* **1996**, *39*, 1227−1235.
(32) Talele, T. T.; Kulkarni, V. M. Three-dimensional quantitative structure−activity relationship (QSAR) and receptor mapping of cytochrome P-450(14 α DM) inhibiting azole antifungal agents. *J. Chem. Inf. Comput. Sci.* **1999**, *39*, 204−210.
(33) Talele, T. T.; Kulkarni, S. S.; Kulkarni, V. M. Development of pharmacophore alignment models as input for comparative molecular field analysis of a diverse set of azole antifungal agents. *J. Chem. Inf. Comput. Sci.* **1999**, *139*, 958−966.
(34) Fukuoka, T.; Johnston, D. A.; Winslow, C. A.; de Groot, M. J.; Burt, C.; Hitchcock, C. A.; Filler, S. G. Genetic basis for differential activities of fluconazole and voriconazole against *Candida krusei*. *Antimicrob. Agents Chemother.* **2003**, *47*, 1213−1219.
(35) Holtje, H. D.; Fattorusso, C. Construction of a model of the *Candida albicans* lanosterol 14-α-demethylase active site using the homology modelling technique. *Pharm. Acta Helv.* **1998**, *72*, 271−277.
(36) Lewis, D. F.; Wiseman, A.; Tarbit, M. H. Molecular modelling of lanosterol 14α-demethylase (CYP51) from *Saccharomyces cerevisiae* via homology with CYP102, a unique bacterial cytochrome P450 isoform: quantitative structure−activity relationships (QSARs) within two related series of antifungal azole derivatives. *J. Enzyme Inhib.* **1999**, *14*, 175−192.
(37) Xiao, L.; Madison, V.; Chau, A. S.; Loebenberg, D.; Palermo, R. E.; McNicholas, P. M. Three-dimensional models of wild-type and mutated forms of cytochrome P450 14α-sterol demethylases from Aspergillus fumigatus and *Candida albicans* provide insights into posaconazole binding. *Antimicrob. Agents Chemother.* **2004**, *48*, 568−574.
(38) Gollapudy, R.; Ajmani, S.; Kulkarni, S. A. Modeling and interactions of Aspergillus fumigatus lanosterol 14-αdemethylase 'A' with azole antifungals. *Bioorg. Med. Chem.* **2004**, *12*, 2937−2950.
(39) Cramer, R. D.; Patterson, D. E.; Bunce, J. D. Comparative molecular field analysis (CoMFA). 1. Effect of shape on binding of steroids to carrier proteins. *J. Am. Chem. Soc.* **1988**, *110*, 5959−5967.
(40) Klebe, G.; Abraham, U.; Mietzner, T. Molecular similarity indices in a comparative analysis (CoMSIA) of drug molecules to correlate and predict their biological activity. *J. Med. Chem.* **1994**, *37*, 4130−4146.
(41) Sheng, C.; Chen, Y.; Zhang, W.; Song, Y.; Ji, H.; Zhou, Y.; Zhu, J.; Lu, J. Optimization of the synthesis of the key intermediateof fluconazole by the orthogonal experimental design. *Zhongguo Yaowu Huaxue Zazhi* **2002**, *12*, 344−346.
(42) Singer, G. M.; Andrews, A. W.; Guo, S. M. Quantitative structure−activity relationship of the mutagenicity of substituted N-nitroso-N-benzylmethylamines: possible implications for carcinogenicity. *J. Med. Chem.* **1986**, *29*, 40−44.
(43) Bringmann, G.; Rummey, C. 3D QSAR investigations on antimalarial naphthylisoquinoline alkaloids by comparative molecular similarity indices analysis (CoMSIA), based on different alignment approaches. *J. Chem. Inf. Comput. Sci.* **2003**, *43*, 304−316.
(44) Bohm, M.; St rzebecher, J.; Klebe, G. Three-dimensional quantitative structure−activity relationship analyses using comparative molecular field analysis and comparative molecular similarity indices analysis to elucidate selectivity differences of inhibitors binding to trypsin, thrombin, and factor Xa. *J. Med. Chem.* **1999**, *42*, 458−477.
(45) Bush, B. L.; Nachbar, R. B., Jr. Sample-distance partial least squares: PLS optimized for many variables, with application to CoMFA. *J. Comput.-Aided Mol. Des.* **1993**, *7*, 587−619.
(46) Luty, B. A.; Wasserman, Z. R.; Stouten, P. F. W.; Hodge, C. N.; Zacharias, M.; McCammon, J. A. A molecular mechanics/grid method for evaluation of ligand−receptor interactions. *J. Comput. Chem.* **1995**, *16*, 454−464.
(47) Bohm, H. J. The development of a simple empirical scoring function to estimate the binding constant for a protein−ligand complex of known three-dimensional structure. *J. Comput.-Aided Mol. Des.* **1994**, *8*, 243−256.
(48) Bohm, H. J. Prediction of binding constants of protein ligands: a fast method for the prioritization of hits obtained from de novo design or 3D database search programs. *J. Comput.-Aided Mol. Des.* **1998**, *12*, 309−323.
(49) Macchiarulo, A.; Costantino, G.; Fringuelli, D.; Vecchiarelli, A.; Schiaffella, F.; Fringuelli, R. 1,4-Benzothiazine and 1,4-benzoxazine imidazole derivatives with antifungal activity: a docking study. *Bioorg. Med. Chem.* **2002**, *10*, 3415−3423.
(50) Lepesheva, G. I.; Virus, C.; Waterman, M. R. Conservation in the CYP51 family. Role of the B′ helix/BC loop and helices F and G in enzymatic function. *Biochemistry* **2003**, *42*, 9091−9101.
(51) SYBYL 6.9: Tripos Associates, Inc. 1699S. Hanley Road, Suite 303, St. Louis, MO 63144. 2003.
(52) InsightII 2000: Molecular Simulation Inc. 9685 Scranton Road, San Diego, CA 92121-3752. 1999.
(53) Cramer, R. D.; Bunce, J. D.; Patterson, D. E. Crossvalidation, bootstrapping and partial least squares compared with multiple regression in conventional QSAR studies. *QSAR* **1988**, *7*, 18−25.
(54) Bohm, H. J. The computer program LUDI: a new method for the de novo design of enzyme inhibitors. *J. Comput.-Aided Mol. Des.* **1992**, *6*, 61−78.

JM051211N